Computer Modeling in Engineering & Sciences

Tech Science Press

https://doi.org/10.32604/cmes.2026.076624

ARTICLE

Natural Frequency-Based Sensitivity Analysis of Pipe Systems with Uncertain Clamp Stiffness and Position Parameters

Yan Shi[1,2], Xin Wang[3], Yi Wang[3], Bingfeng Zhao[4], Shang Ren[4] and Xufang Zhang[4,*]

[1]National Elite Institute of Engineering, Northwestern Polytechnical University, Xi'an, China
[2]Shenyang Liming Aero Engine Corporation Limited, Aero Engine Corporation of China, Shenyang, China
[3]Shenyang Engine Research Institute, Aero Engine Corporation of China, Shenyang, China
[4]School of Mechanical Engineering and Automation, Northeastern University, Shenyang, China

*Corresponding Author: Xufang Zhang. Email: zhangxf@mail.neu.edu.cn

Received: 23 November 2025; Accepted: 04 February 2026; Published: 30 March 2026

ABSTRACT: This paper introduces a computationally efficient global sensitivity analysis method for quantifying the influence of uncertain clamp support conditions on the natural frequencies of aero-engine pipe systems. The dynamic model is based on a three-dimensional Timoshenko beam finite element formulation, with clamps represented as distributed spring elements possessing anisotropic stiffness. To overcome the prohibitive cost of traditional Monte Carlo simulation, the multiplicative dimensional reduction method (M-DRM) is integrated with variance decomposition theory. This approach approximates the high-dimensional frequency response function as a product of univariate components, enabling rapid computation of Sobol' sensitivity indices with a computational cost reduced by three orders of magnitude. Numerical case studies on a planar Z-shaped pipe and a spatial series-parallel configuration reveal that clamp position parameters dominate the system's natural frequency characteristics. For critical clamps, Sobol' indices exceed 0.8 across multiple vibration modes, whereas stiffness parameters exhibit negligible influence. The proposed methodology provides a rigorous and efficient tool for identifying dominant uncertainty sources, guiding tolerance allocation in manufacturing, and informing robust support design for vibration-sensitive piping systems.

KEYWORDS: Natural frequencies; multiplicative dimensionality reduction method; sobol' index; clamp-pipe systems

1 Introduction

External pipe systems are critical components in aero-engine architectures, responsible for transporting hydraulic fluid, fuel, lubricating oil, and compressed air [1,2]. Their dynamic behavior directly influences structural integrity and reliability, as excessive vibrations can lead to clamp loosening, fatigue cracking, and progressive structural failure. Clamps act as elastic supports that define the boundary conditions of pipe segments, thereby shaping the system's natural frequencies and mode shapes. Variations in clamp stiffness alter the constraint level and shift eigenfrequencies. Furthermore, uncertainties in clamp installation position, such as axial misalignments or angular offsets, introduce asymmetry in mass and stiffness distribution [3,4]. These spatial deviations affect eigenfrequency predictions and may induce unexpected resonances [5–7].

Extensive research has focused on dynamic modeling of clamp-pipe systems. Widely adopted methods include the finite-element method [8,9], the spectral element method [10,11], the transfer matrix method [12–15], and semi-analytical methods [16–19]. These techniques enable comprehensive modal analysis under diverse boundary conditions. For instance, ref. [20] proposed an enhanced spectral element method for

handling complex clamped boundaries, ref. [21] introduced an improved high-efficiency transfer matrix method for fluid-conveying pipes, and ref. [22] combined spectral and transfer matrix methods to study acoustic black hole piping structures. While effective in specific applications, these methods face challenges in balancing computational efficiency with high-fidelity modeling for complex three-dimensional pipe systems involving multiple uncertain clamp parameters. The Timoshenko beam based finite element model is particularly suitable for this study because it accurately captures shear deformation and rotary inertia effects, enabling precise representation of dynamic stiffness under varying clamp conditions. This formulation supports reliable prediction of natural frequencies and mode shapes, and its flexibility facilitates the incorporation of clamp parameters for sensitivity analysis.

The vibration characteristics of a clamp-pipe system represent an implicit function of clamp parameters. Previous studies have developed simulation models based on experimentally tested stiffness coefficients [23], employed distributed spring elements to model elastic support [24], and used Euler-Bernoulli beam elements with springs for multi-clamp systems [25]. Building on these foundations, this study adopts a Timoshenko beam finite element model combined with spring elements to characterize elastic support, providing an efficient computational approach for sensitivity analysis with uncertain clamp parameters. To quantitatively assess the impact of uncertain factors, sensitivity analysis methods are essential. These methods are categorized into local and global sensitivity analyses [26,27]. Local sensitivity analysis employs gradient-based metrics to evaluate parameter influence at specific points [28]. For example, ref. [29] used the Taguchi method for aircraft landing gear shimmy analysis, and [30] conducted parameter perturbation analysis for pipe systems. However, local sensitivity analysis provides only local approximations and requires gradient computations, limiting its application to complex implicit functions such as natural frequencies [31].

Global sensitivity analysis quantifies parameter influence across their entire domain [32,33]. Applications include aerospace gear systems [34], air rudder flutter [35], bridge dynamics [36], and multi-span pipe resonance [37]. The Sobol' method, based on variance decomposition theory, quantifies the influence of individual inputs and their interactions on structural vibrations [38,39]. It overcomes the reference-point dependence of local approaches by capturing contributions across the complete parameter domain. The first-order index S_i measures the main effect of input X_i, while the total-effect index S_{Ti} includes all interactions involving X_i. This provides comprehensive identification of dominant parameters with quantitative interpretability. The core computational challenge in Sobol' analysis involves evaluating conditional expectations of the model response. Monte Carlo simulation is commonly used but requires substantial computational resources due to slow convergence [40]. For complex three-dimensional pipe systems with multiple uncertain clamp parameters, direct Monte Carlo simulation becomes computationally prohibitive.

The multiplicative dimensional reduction method offers an efficient alternative [41]. It derives approximate analytical solutions for Sobol' indices through a finite number of operations by decomposing the input-output relationship into multiplicative terms. This significantly reduces the sampling burden while preserving accuracy. The multiplicative dimensional reduction method has demonstrated broad applicability, including uncertainty quantification in MEMS actuators [42], gas synthesis processes [43], and nonlinear structural dynamics [44]. This study addresses the vibration characteristics of aero-engine pipe systems under uncertain support conditions. Practical installation involves unavoidable variations in clamp positioning and stiffness due to manufacturing tolerances and assembly processes. These uncertainties cause natural frequency shifts, potentially leading to resonance and structural failure. The objective is to develop an efficient sensitivity analysis method that identifies critical clamp parameters, guiding tolerance design and installation quality control for enhanced reliability.

The proposed methodology integrates three principal technical components, namely a three-dimensional Timoshenko beam finite-element model for dynamic simulation, the multiplicative

dimensional reduction method for efficient uncertainty propagation, and Sobol' indices for global sensitivity quantification. This integration preserves the accuracy inherent in three-dimensional beam theory while achieving significant computational efficiency through dimensional reduction. The balanced fulfillment of accuracy and efficiency renders the method particularly suitable for the analysis of aero-engine pipe systems, where both attributes are critically demanded in practical engineering applications.

The remainder of this paper is organized as follows. Section 2 develops the simulation model using three-dimensional Timoshenko beam theory. Section 3 presents the Sobol' sensitivity indices and the multiplicative dimensional reduction method approximation for efficient computation. Section 4 provides numerical examples for planar and spatial pipe systems. Finally, Section 5 summarizes the main conclusions.

2 Model for Dynamic Analysis of the Clamp-Pipe System

To ensure the accuracy and reliability of sensitivity analysis for natural vibration characteristics in complex piping systems, this study develops a parametric geometric model that captures both nominal configurations and realistic installation variations. The model enables precise representation of spatial pipe layouts, including straight segments, bends, and support constraints, forming the basis for a comprehensive dynamic analysis framework. By integrating spring elements to simulate clamp-induced elastic supports and employing a hybrid beam-spring finite element formulation, the approach provides a robust foundation for global sensitivity assessment of system-level dynamic responses. This section presents the analytical framework for modeling the natural vibration behavior of pipe systems under varying geometric and boundary conditions.

2.1 The Timoshenko Beam Based Pipe Element

Consider a hollow circular pipe segment of length L with outer diameter D and inner diameter d. A local coordinate system (x, y, z) is defined for each segment. Within the finite element framework, the pipe is discretized into elements, with each node possessing six degrees of freedom: three translational displacements (u, v, w) along the local axes and three rotational displacements $(\theta_x, \theta_y, \theta_z)$ about these axes. The corresponding mechanical model based on Timoshenko beam theory is illustrated in Fig. 1.

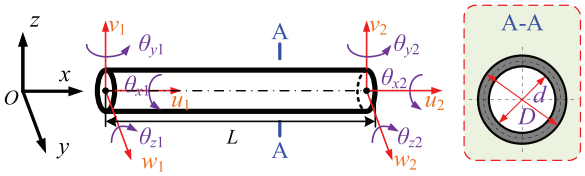

Figure 1: A mechanical model of pipes based on Timoshenko beam.

The geometric parameters of the pipe, including outer diameter D, inner diameter d, and length L, are determined based on typical aero-engine fuel and hydraulic pipe specifications. The material properties, such as Young's modulus E, density ρ, and Poisson's ratio ν, are selected according to the commonly used stainless steel (e.g., AISI 304) for aerospace piping systems. These values are representative of actual engine components and ensure the model captures realistic dynamic behavior. The shear correction factor κ is set to 0.9 for circular thin-walled pipes, accurately accounting for shear deformation effects in Timoshenko beam theory. The selection of these parameters aligns with industry standards and prior experimental studies on similar pipe systems.

Based on the Timoshenko beam theory, the complete element displacement vector $\mathbf{q}_e$ for the element connecting nodes 1 and 2 is defined as

$$\mathbf{q}_e = [u_1, v_1, w_1, \theta_{x1}, \theta_{y1}, \theta_{z1}, u_2, v_2, w_2, \theta_{x2}, \theta_{y2}, \theta_{z2}]^{\mathrm{T}}. \tag{1}$$

The kinetic energy for the pipe segment is theoretically represented as

$$T_e = \frac{1}{2}\int_0^L \left[\rho A\left(\dot{u}^2 + \dot{v}^2 + \dot{w}^2\right) + \rho I_y \dot{\theta}_y^2 + \rho I_z \dot{\theta}_z^2 + \rho J \dot{\theta}_x^2\right] \mathrm{d}x, \tag{2}$$

where ρ is the material density, A is the cross-sectional area, i.e., $A = \frac{\pi}{4}(D^2 - d^2)$, whereas I_y and I_z are the second moments of area about the y- and z-axes, respectively. For the circle-section based pipe element, one has $I_y = I_z = \frac{\pi}{64}(D^4 - d^4)$, and the polar moment of inertia J is given as $J = \frac{\pi}{32}(D^4 - d^4)$, in which d and D define the inner and outer diameters of the pipe segment, respectively.

The strain energy of the Timoshenko beam based pipe element is defined as

$$U_e = \frac{1}{2}\int_0^L \left[EAu'^2 + EI_y\theta_y'^2 + EI_z\theta_z'^2 + GJ\theta_x'^2 + \kappa GA(v' - \theta_z)^2 + \kappa GA(w' + \theta_y)^2\right]\mathrm{d}x, \tag{3}$$

where E is the Young's modulus, κ is the shear correction factor. Together with the Poisson ratio parameter ν, one can define the shear modulus as $G = \frac{E}{2(1+\nu)}$.

Application of Hamilton's principle, $\delta\int_{t_1}^{t_2}(T_e - U_e)\mathrm{d}t = 0$, to the pipe segment derives the element-based equation for dynamic motion of the Timoshenko beam based pipe element

$$\mathbf{M}_e\ddot{\mathbf{q}}_e + \mathbf{K}_e\mathbf{q}_e = \mathbf{0}. \tag{4}$$

In this formulation, the element mass and stiffness matrices $\mathbf{M}^e$ and $\mathbf{K}^e$ for the Timoshenko beam element govern the interactions among the twelve local degrees of freedom in $\mathbf{q}_e$, and are given by

$$\mathbf{M}_e = \begin{bmatrix} \mathbf{M}_{11}^e & \mathbf{M}_{12}^e \\ \mathbf{M}_{21}^e & \mathbf{M}_{22}^e \end{bmatrix} \quad \text{and} \quad \mathbf{K}_e = \begin{bmatrix} \mathbf{K}_{11}^e & \mathbf{K}_{12}^e \\ \mathbf{K}_{21}^e & \mathbf{K}_{22}^e \end{bmatrix}, \tag{5}$$

where $(\cdot)_{11}^e$ and $(\cdot)_{22}^e$ characterize the self-dependency of the degrees of freedom at nodes 1 and 2, respectively, while $(\cdot)_{12}^e = (\cdot)_{21}^e$ captures the coupling between the two nodes. Detailed expressions for the mass and stiffness matrices can be found in Appendix A.

The Timoshenko beam element incorporates six degrees of freedom per node: three translational and three rotational displacements. This formulation enables accurate representation of three-dimensional pipe behavior. The consistent derivation of kinetic and strain energy expressions captures rotary inertia effects and transverse shear deformation of the pipe body. This formulation serves as the foundation for subsequent global sensitivity analysis, enabling investigation of how clamp support parameters influence the inherent vibrational characteristics of complex piping systems.

2.2 Modeling of Single Clamps

Single clamps are extensively employed in aerospace and industrial piping systems to fix pipe segments to engine casings or structural frames. As critical boundary conditions, they substantially influence the system's dynamic behavior, particularly its natural frequency distribution and mode shapes. Manufacturing tolerances, installation variability, and geometric asymmetry often lead to directional dependence and non-uniformity in clamp stiffness properties, resulting in anisotropic support behavior. Accurate modeling

of these effects is crucial for predicting vibration response, avoiding resonance, and ensuring structural reliability under operational loads. This section presents a finite element based approach to model the elastic support of single clamps, incorporating translational and rotational stiffness across six degrees of freedom to capture their asymmetric mechanical response.

As illustrated in Fig. 2, the elastic support behavior of a single clamp is modeled using two sets of spring elements connected at the node corresponding to the clamp location. These springs represent the translational and rotational stiffness characteristics of the clamp across six degrees of freedom: k_x^{SC}, k_y^{SC}, k_z^{SC} for translational stiffness along the x-, y-, and z-axes, and $k_{\theta_x}^{\mathrm{SC}}$, $k_{\theta_y}^{\mathrm{SC}}$, $k_{\theta_z}^{\mathrm{SC}}$ for rotational stiffness about these axes. The directional variation of these stiffness coefficients reflects the anisotropic nature of the clamp's geometric asymmetry and bolted mounting configuration, which results from manufacturing tolerances and installation constraints.

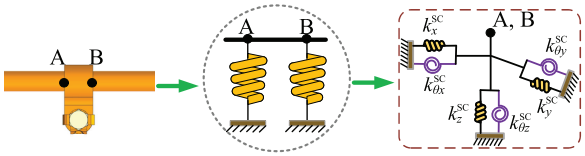

Figure 2: Mechanical model for dynamic simulation of single clamp.

Each node-localized spring group is represented by a diagonal stiffness matrix

$$\mathbf{K}_{\mathrm{SC}} = \frac{1}{2} \times \mathrm{diag}\left(k_x^{\mathrm{SC}}, k_y^{\mathrm{SC}}, k_z^{\mathrm{SC}}, k_{\theta_x}^{\mathrm{SC}}, k_{\theta_y}^{\mathrm{SC}}, k_{\theta_z}^{\mathrm{SC}}\right). \tag{6}$$

In the finite element assembly process, the factor 1/2 distributes the elastic support of a clamp equally between its two adjacent nodes, such as Points A and B in Fig. 2. This represents the spatial distribution of clamp stiffness along the pipe span, with the total stiffness of the clamp assembly divided evenly between its connection points.

In summary, the presented method enables precise capture of the elastic support behavior of single clamps within the finite element model. By integrating experimentally derived stiffness parameters and a physically consistent spring-mass formulation, the method supports accurate prediction of natural frequencies, mode shapes, and sensitivity to parametric variations of the single clamp. This capability is particularly valuable in engineering applications where clamp stiffness and position are treated as uncertain variables, enabling robust dynamic analysis and informed decision-making in the early stages of system design.

2.3 Modeling of Double Clamps

Double clamps are widely used in aerospace and industrial piping systems to provide enhanced structural restraint at critical junctions between adjacent pipe segments. To capture their dynamic influence within the finite element environment, double clamps are modeled as discrete connection mechanisms linking two nodes on adjacent pipe segments. The mechanical properties are represented by concentrated masses and stiffnesses distributed at the connection points as depicted in Fig. 3. The superscript CE distinguishes double clamp parameters from those of other components, facilitating clear identification and efficient model management.

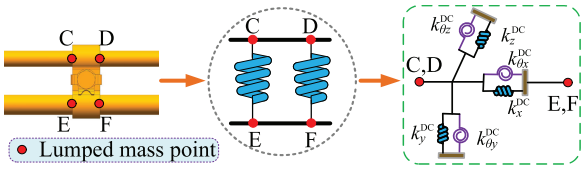

Figure 3: A mechanical model for dynamic simulation of double clamps.

The mass contribution of the double clamp is distributed equally among its four attachment points, two per node, reflecting the symmetric nature of its installation. As a result, each nodal mass represents one-quarter of the total double clamp mass m_{CE}. The corresponding mass matrix is constructed as a block-diagonal matrix

$$\mathbf{M}_{\mathrm{CE}}^{e} = \begin{bmatrix} \mathbf{M}_{11}^{\mathrm{CE}} & \mathbf{0}_{6\times6} \\ \mathbf{0}_{6\times6} & \mathbf{M}_{22}^{\mathrm{CE}} \end{bmatrix}, \tag{7}$$

where $\mathbf{M}_{11}^{\mathrm{CE}} = \mathbf{M}_{22}^{\mathrm{CE}} = \frac{1}{4} \times \mathrm{diag}(m_{\mathrm{CE}}, m_{\mathrm{CE}}, m_{\mathrm{CE}}, 0, 0, 0)$ accounts for the lumped translational inertia at each connection point. The model neglects the rotational inertia of the clamp, a standard simplification in the dynamic analysis of beam-like structures supported by discrete fixtures. This assumption is physically justified because the rotational inertia of a compact clamp mass is typically negligible compared to that of the pipe segments, which possess significantly larger radii of gyration. Consequently, the inertial coupling introduced by clamp rotation has a minimal effect on the global system dynamics, particularly for the lower-order modes which are the primary focus of this sensitivity study. This approach aligns with conventional modeling practices, streamlining the finite element formulation without compromising the reliability of the identified parameter importance rankings.

The stiffness matrix of the double clamp reflects the coupling between the two connected nodes. It is defined in a full 12 × 12 block form to account for mutual interactions

$$\mathbf{K}_{\mathrm{CE}}^{e} = \begin{bmatrix} \mathbf{K}_{11}^{\mathrm{CE}} & \mathbf{K}_{12}^{\mathrm{CE}} \\ \mathbf{K}_{21}^{\mathrm{CE\,T}} & \mathbf{K}_{22}^{\mathrm{CE}} \end{bmatrix}, \tag{8}$$

with submatrices given by

$$\begin{cases} \mathbf{K}_{11}^{\mathrm{CE}} = \frac{1}{2} \times \mathrm{diag}(k_x^{\mathrm{CE}}, k_y^{\mathrm{CE}}, k_z^{\mathrm{CE}}, k_{\theta x}^{\mathrm{CE}}, k_{\theta y}^{\mathrm{CE}}, k_{\theta z}^{\mathrm{CE}}) \\ \mathbf{K}_{22}^{\mathrm{CE}} = \frac{1}{2} \times \mathrm{diag}(k_x^{\mathrm{CE}}, k_y^{\mathrm{CE}}, k_z^{\mathrm{CE}}, k_{\theta x}^{\mathrm{CE}}, k_{\theta y}^{\mathrm{CE}}, k_{\theta z}^{\mathrm{CE}}) \\ \mathbf{K}_{12}^{\mathrm{CE}} = -\frac{1}{2} \times \mathrm{diag}(k_x^{\mathrm{CE}}, k_y^{\mathrm{CE}}, k_z^{\mathrm{CE}}, k_{\theta x}^{\mathrm{CE}}, k_{\theta y}^{\mathrm{CE}}, k_{\theta z}^{\mathrm{CE}}). \end{cases} \tag{9}$$

Here, k_x^{CE}, k_y^{CE}, k_z^{CE} denote the translational stiffness coefficients, while $k_{\theta x}^{\mathrm{CE}}$, $k_{\theta y}^{\mathrm{CE}}$, $k_{\theta z}^{\mathrm{CE}}$ represent the rotational stiffness values, all derived from the mechanical properties of the clamp material and geometric design. The negative off-diagonal blocks indicate that displacement at one node induces an opposing reaction at the other, consistent with the principle of action and reaction.

In summary, this procedure enables accurate representation of double clamp effects on the system dynamic characteristics. By incorporating both mass and stiffness contributions in a physically consistent manner, the model provides reliable prediction of natural frequencies and mode shapes for complex piping systems. The resulting element-level matrices are assembled into the global system equations, enabling comprehensive evaluation of how double clamp installations influence overall pipe dynamic behavior.

2.4 System Model for Natural Frequency Analysis

The integration of Timoshenko beam finite element modeling with discrete clamp representations enables a comprehensive and physically consistent procedure for analyzing the dynamic behavior of clamp-pipe systems. This section presents the global system formulation that combines contributions from pipe segments, single clamps, and double clamps into unified mass and stiffness matrices. The resulting model captures the influence of both clamp stiffness and position on the natural frequencies and mode shapes of the system, providing a robust foundation for sensitivity analysis and design optimization. In this study, the focus is on the deterministic modal characteristics of the clamp-pipe system, specifically the first five natural frequencies, which are critical for identifying potential resonance risks in engineering applications.

The Timoshenko beam finite element procedure allows one to obtain the global matrices for dynamic modeling of the clamp-pipe system as follows:

$$\begin{cases} \mathbf{K} = \sum\limits_{\forall e} \mathbf{T}_e^{\mathrm{T}} \mathbf{K}_{\mathrm{Pipe}}^{e} \mathbf{T}_e + \sum\limits_{\forall e} \mathbf{T}_e^{\mathrm{T}} \mathbf{K}_{\mathrm{SC}}^{e} \mathbf{T}_e + \sum\limits_{\forall e} \mathbf{T}_e^{\mathrm{T}} \mathbf{K}_{\mathrm{CE}}^{e} \mathbf{T}_e \\ \mathbf{M} = \sum\limits_{\forall e} \mathbf{T}_e^{\mathrm{T}} \mathbf{M}_{\mathrm{Pipe}}^{e} \mathbf{T}_e + \sum\limits_{\forall e} \mathbf{T}_e^{\mathrm{T}} \mathbf{M}_{\mathrm{CE}}^{e} \mathbf{T}_e. \end{cases} \tag{10}$$

Herein, $\mathbf{K}_{\mathrm{Pipe}}^{e}$ and $\mathbf{M}_{\mathrm{Pipe}}^{e}$ denote the element-level stiffness and mass matrices of the pipe segment formulated based on Timoshenko beam theory with appropriate shape functions. The terms $\mathbf{K}_{\mathrm{SC}}^{e}$ and $\mathbf{M}_{\mathrm{SC}}^{e}$ represent the stiffness and mass contributions from single clamps embedded at specific nodal locations according to their installation configuration. Similarly, $\mathbf{K}_{\mathrm{CE}}^{e}$ and $\mathbf{M}_{\mathrm{CE}}^{e}$ account for the coupled stiffness and inertial effects introduced by double clamps, which span between two distinct nodes and are applied as full 12×12 matrices during assembly. The summation operator $\sum_{\forall e}(\cdot)$ denotes the standard finite element procedure, which maps each element's contribution to its correct position in the global system matrices, preserving connectivity and continuity across the entire structure. The transformation matrix $\mathbf{T}_e$ is constructed by repeating the directional cosine matrix $\mathbf{t}_e$ four times along the block diagonal:

$$\mathbf{T}_e = \mathrm{blkdiag}(\mathbf{t}_e, \mathbf{t}_e, \mathbf{t}_e, \mathbf{t}_e). \tag{11}$$

The operator $\mathrm{blkdiag}(\cdot)$ creates a block-diagonal matrix, and $\mathbf{t}_e$ defines the orientation of the local coordinate system relative to the global frame:

$$\mathbf{t}_e = \begin{bmatrix} \cos(x,u) & \cos(y,u) & \cos(z,u) \\ \cos(x,v) & \cos(y,v) & \cos(z,v) \\ \cos(x,w) & \cos(y,w) & \cos(z,w) \end{bmatrix}, \tag{12}$$

where (u, v, w) denote the local coordinate axes and (x, y, z) the global axes. The columns of $\mathbf{t}_e$ are the local unit vectors $\mathbf{v}_u, \mathbf{v}_v, \mathbf{v}_w$ expressed in the global coordinate system.

The natural frequencies of the clamp-pipe system are computed by solving the generalized eigenvalue problem, which establishes an implicit relationship between the system response and clamp parameters. The natural frequency vector $\mathbf{Y} = [y_1, y_2, \cdots, y_n]^{\mathrm{T}}$ depends on the parameter vector $\mathbf{x} = [x_1, x_2, \cdots, x_m]^{\mathrm{T}}$, which contains clamp stiffness coefficients and spatial coordinates. Each parameter in $\mathbf{x}$ represents either a clamp location or a translational or rotational stiffness coefficient, thus capturing geometric installation variations and material property effects. This parametric formulation enables systematic investigation of how uncertainties in clamp configurations propagate through the system and influence the dynamic response.

The modal properties are obtained by solving the generalized eigenvalue problem

$$\mathbf{K}(\mathbf{x})\boldsymbol{\phi}^{(i)}(\mathbf{x}) = \Omega_i^2(\mathbf{x})\mathbf{M}(\mathbf{x})\boldsymbol{\phi}^{(i)}(\mathbf{x}) \quad (i = 1, 2, \cdots, n), \tag{13}$$

where $\Omega_i(\mathbf{x})$ and $\boldsymbol{\phi}^{(i)}(\mathbf{x})$ denote the ith natural frequency and mode shape, respectively, both explicitly dependent on the clamp parameter vector $\mathbf{x}$. The global mass matrix $\mathbf{M}(\mathbf{x})$ and stiffness matrix $\mathbf{K}(\mathbf{x})$ are assembled according to Section 2.4, with entries that are functions of the clamp configuration parameters. This parametric model provides a comprehensive framework for evaluating the influence of clamp stiffness and positioning uncertainties on the system's vibrational characteristics, particularly the first several dominant modes that govern dynamic behavior under operational conditions.

In summary, this section presents a dynamic model for natural frequency analysis of clamp-pipe systems, integrating three-dimensional Timoshenko beam theory with discrete clamp representations. Pipe segments are modeled using Timoshenko beam finite elements, capturing bending and shear deformation effects essential for accurate dynamic characterization of aero-engine piping components. Clamps are represented as distributed spring elements that account for directional stiffness variations and anisotropic support behavior. Double clamps are modeled as coupled connection mechanisms introducing stiffness coupling between adjacent nodes. This integrated model establishes an explicit parametric relationship between clamp configuration parameters and system natural frequencies, forming a computational foundation for subsequent sensitivity analysis. The model enables evaluation of how clamp stiffness coefficients and spatial positioning influence the vibrational characteristics of complex piping systems, with emphasis on the dominant modes critical for resonance avoidance.

3 Global Sensitivity Analysis of Natural Frequencies with Respect to Clamp Parameters

Uncertainties in clamp installation, including positional deviations and stiffness variations of single and double clamps, significantly influence the dynamic behavior of engine piping systems. These uncertainties originate from manufacturing tolerances, assembly errors, thermal expansion, and material property fluctuations during operation. Consequently, the natural frequencies and mode shapes of the system exhibit variability, potentially leading to unexpected resonance or excessive vibration under operational loads. Sensitivity analysis quantifies the impact of these uncertain parameters on the system dynamic response, identifying dominant factors and guiding robust design practices. This section presents a comprehensive procedure for analyzing the sensitivity of natural vibration characteristics to clamp position deviations and stiffness parameters, employing global sensitivity indices derived from variance decomposition, multiplicative dimension-reduction modeling, and Monte Carlo simulation.

3.1 The Sobol' Sensitivity Index

The natural frequency response of the clamp-pipe system is characterized by the functional relationship $y_k = \mathcal{M}_k(\mathbf{x})$ $(k = 1, \cdots, n)$, where y_k is the k-th natural frequency and $\mathbf{x} = [x_1, x_2, \ldots, x_m]^{\mathrm{T}}$ is the input vector containing clamp stiffness coefficients and positional coordinates. This parametric model enables systematic evaluation of how uncertainties in clamp configurations propagate to the system's dynamic characteristics.

Sobol' sensitivity analysis decomposes the output variance into contributions from individual parameters and their interactions. The main-effect sensitivity index for parameter x_i quantifies its individual contribution to the total output variance, defined as

$$S_{i,k} = \frac{V\left[E_{\mathbf{x}_{-i}}[\mathcal{M}_k(\mathbf{x}) \mid x_i]\right]}{V[\mathcal{M}_k(\mathbf{x})]} \quad (i = 1, \cdots, m), \tag{14}$$

where $\mathbf{x}_{-i}$ denotes all input variables except x_i, and $E_{\mathbf{x}_{-i}}[\cdot]$ is the conditional expectation over $\mathbf{x}_{-i}$.

The total-effect sensitivity index accounts for both the main effect of x_i and all its interactions with other parameters, defined as

$$S_{\mathrm{T}i,k} = \frac{E_{\mathbf{x}_{-i}}\left[V_{x_i}[\mathcal{M}_k(\mathbf{x}) \mid \mathbf{x}_{-i}]\right]}{V[\mathcal{M}_k(\mathbf{x})]} \quad (i = 1, \cdots, m), \tag{15}$$

where $V_{x_i}[\mathcal{M}_k(\mathbf{x}) \mid \mathbf{x}_{-i}]$ is the conditional variance of the response given $\mathbf{x}_{-i}$.

These sensitivity indices enable quantitative assessment of how clamp stiffness and position uncertainties influence the natural frequency characteristics of piping systems. The first-order index $S_{i,k}$ measures the direct effect of x_i on the k-th natural frequency, while the total-effect index $S_{\mathrm{T}i,k}$ captures all interactions involving x_i, providing comprehensive identification of dominant clamp parameters governing system dynamic behavior.

Exact computation of Sobol indices requires evaluating high-dimensional conditional expectations, posing significant computational challenges for complex pipe system models. For clamp-pipe systems with numerous uncertain parameters representing clamp stiffness coefficients and positional coordinates, direct Monte Carlo simulation becomes computationally prohibitive due to its inherent double-loop sampling structure.

To estimate the sensitivity indices via Monte Carlo simulation, two independent sample matrices $\mathbf{X}^{(1)}$ and $\mathbf{X}^{(2)}$ are generated from the input parameter space, each of dimension $N \times m$, where m is the number of uncertain clamp parameters. For each sample, the natural frequency response $y_{k,j}^{(i)} = \mathcal{M}_k(\mathbf{x}_j^{(i)})$ is computed using the dynamic model from Section 2, requiring $2N$ finite element evaluations.

The main computational burden arises from evaluating the conditional expectation $E_{\mathbf{x}_{-i}}[\mathcal{M}_k(\mathbf{x}) \mid x_i = x_{i,j}]$, which requires constructing modified sample matrices. In these matrices, the i-th column is fixed at $x_{i,j}$ while all other columns are taken from $\mathbf{X}^{(2)}$. This double-loop structure requires N additional finite element analyses per parameter, leading to $2N + mN$ model evaluations for the first-order sensitivity indices of all m parameters for a single natural frequency. The conditional expectation estimator is

$$\hat{E}_{\mathbf{x}_{-i}}\left[\mathcal{M}_k(\mathbf{x}) \mid x_i = x_{i,j}\right] = \frac{1}{N}\sum_{l=1}^{N} \mathcal{M}_k\left(x_{i,j}, \mathbf{x}_{l,-i}^{(2)}\right), \tag{16}$$

where $\mathbf{x}_{l,-i}^{(2)}$ is the l-th row of $\mathbf{X}^{(2)}$ with the i-th element removed.

The main-effect sensitivity index is estimated as

$$\hat{S}_{i,k} = \frac{\frac{1}{N}\sum_{j=1}^{N}\left(\hat{E}_{\mathbf{x}_{-i}}\left[\mathcal{M}_k(\mathbf{x}) \mid x_i = x_{i,j}\right] - \bar{y}_k\right)^2}{\frac{1}{N}\sum_{j=1}^{N}\left(y_{k,j}^{(1)} - \bar{y}_k\right)^2}, \tag{17}$$

with $\bar{y}_k = \frac{1}{N}\sum_{j=1}^{N} y_{k,j}^{(1)}$ as the sample mean of the first response set.

For the total effect, the conditional variance estimator requires computing

$$\hat{V}_{\mathrm{T}i,k} = \frac{1}{N}\sum_{j=1}^{N}\left(\mathcal{M}_k(\mathbf{x}_j^{(1)}) - \hat{E}_{\mathbf{x}_{-i}}\left[\mathcal{M}_k(\mathbf{x}) \mid x_i = x_{i,j}\right]\right)^2, \tag{18}$$

and the total sensitivity index is estimated as

$$\hat{S}_{\mathrm{T}i,k} = \frac{\hat{V}_{\mathrm{T}i,k}}{\hat{V}_{y_k}}, \tag{19}$$

where $\hat{V}_{y_k} = \frac{1}{N}\sum_{j=1}^{N}\left(y_{k,j}^{(1)} - \bar{y}_k\right)^2$ is the sample variance.

This computationally intensive procedure becomes intractable for realistic pipe system models, where each finite element analysis involves assembling and solving the full eigenvalue problem for three-dimensional Timoshenko beam elements with complex clamp boundary conditions. For typical aerospace piping systems with m uncertain clamp parameters and sample size N, the total computational cost for evaluating the first-order index is $N(1+m)$ finite element analyses. For instance, with $m = 10$ and $N = 10^4$, the cost exceeds 10^5 finite element analyses. Such requirements exceed practical engineering limitations, as each finite element analysis may require several seconds to minutes, making brute-force Monte Carlo simulation computationally prohibitive for sensitivity analysis of realistic aerospace piping applications.

3.2 Efficient Computation of Sensitivity Indices Using M-DRM

To overcome the computational challenges associated with direct integration in global sensitivity analysis, the multiplicative dimension reduction method provides an efficient alternative for estimating Sobol indices in complex pipe system models.

The multiplicative dimension reduction method leverages a multiplicative decomposition of the original model response $\mathcal{M}_k(\mathbf{x})$ as [33]

$$\mathcal{M}_k(\mathbf{x}) \approx \mathcal{M}_k(\mathbf{x}_0)^{1-m} \cdot \prod_{i=1}^{m} \mathcal{M}_{k,i}(x_i, \mathbf{x}_{0,-i}). \tag{20}$$

Herein, $\mathbf{x}_0$ is a reference point in the input space, and $\mathbf{x}_{0,-i}$ represents all components of $\mathbf{x}_0$ except x_i.

The component function $\mathcal{M}_{k,i}(x_i, \mathbf{x}_{0,-i})$ is defined as the one-dimensional function obtained by fixing all other variables at their reference values $\mathbf{x}_{0,-i}$ while varying only x_i. Mathematically, $\mathcal{M}_{k,i}(x_i, \mathbf{x}_{0,-i}) = \mathcal{M}_k(x_i, \mathbf{x}_{0,-i})$, where $(x_i, \mathbf{x}_{0,-i})$ denotes the vector with the i-th component equal to x_i and all other components equal to those in $\mathbf{x}_0$. This construction transforms the m-dimensional integration problem into m separate one-dimensional integrals, each evaluated along a single parameter dimension while keeping other parameters fixed at their reference values. The accuracy of this decomposition relies on the assumption that the response function can be approximated as a product of univariate functions, which holds well for natural frequency functions with moderate parameter interactions. This multiplicative structure transforms high-dimensional integrals into products of one-dimensional components, enabling efficient evaluation of the required statistical moments for clamp stiffness and position parameters.

The reference point $\mathbf{x}_0$ is typically chosen as the mean or median of the input distribution. The accuracy of the multiplicative dimensional reduction method approximation depends on the smoothness of the response function and the distance of $\mathbf{x}_0$ from regions of strong nonlinearity. For the natural frequency functions in this study, which are generally smooth with respect to clamp parameters, selecting $\mathbf{x}_0$ at the mean of the input distribution provides good accuracy, as validated by comparison with direct Monte Carlo simulation in our numerical examples.

The first-order moment of the i-th component for the k-th natural frequency is defined as

$$\rho_{i,k} = \mathbb{E}_{X_i}\left[\mathcal{M}_{k,i}(x_i, \mathbf{x}_{0,-i})\right] \quad (i = 1, \cdots, m; k = 1, \cdots, n) \tag{21}$$

and the second-order moment is

$$\theta_{i,k} = \mathbb{E}_{X_i}\left[\mathcal{M}^2_{k,i}(x_i, \mathbf{x}_{0,-i})\right] \quad (i = 1, \cdots, m; k = 1, \cdots, n). \tag{22}$$

These moments can be efficiently computed using Gauss-quadrature integration over the one-dimensional domain of x_i, avoiding the need for expensive multidimensional numerical integration in the sensitivity analysis of pipe natural frequencies.

The numerical integration employs Gaussian quadrature rules with appropriately selected abscissas and weights for evaluating the one-dimensional component functions arising from the multiplicative decomposition. For a p-point Gauss-Legendre quadrature scheme, the integral of the component function $\mathcal{M}_{k,i}(x_i, \mathbf{x}_{0,-i})$ over the standard interval is approximated as

$$\int_{X_i} \mathcal{M}_{k,i}(x_i, \mathbf{x}_{0,-i})\, \mathrm{d}x_i \approx \sum_{l=1}^{p} w_l \mathcal{M}_{k,i}(z_l, \mathbf{x}_{0,-i}) \quad (i = 1, \cdots, m), \tag{23}$$

where z_l and w_l denote the quadrature points and corresponding weights, respectively. Variable transformations are applied to map the original parameter domains to the standard integration interval, enabling consistent application of the quadrature rules across different parameter types [45].

Therefore, the main effect sensitivity index for the i-th parameter corresponding to the k-th natural frequency is estimated as

$$S_{i,k} = \frac{\theta_{i,k}/\rho^2_{i,k} - 1}{\left(\prod_{j=1}^{m} \theta_{j,k}/\rho^2_{j,k}\right) - 1} \quad (i = 1, \cdots, m; k = 1, \cdots, n). \tag{24}$$

Similarly, the total effect sensitivity index, which accounts for both main and interaction effects involving x_i, is given by

$$S_{\mathrm{T}i,k} = \frac{1 - \rho^2_{i,k}/\theta_{i,k}}{1 - \left(\prod_{j=1}^{m} \rho^2_{j,k}/\theta_{j,k}\right)} \quad (i = 1, \cdots, m; k = 1, \cdots, n). \tag{25}$$

The computational efficiency of the multiplicative dimensional reduction method is achieved through systematic reduction of finite element reanalysis requirements. For a system with m uncertain clamp parameters and p-point quadrature, the total number of finite element evaluations required is mp for computing the first-order and total Sobol' sensitivity indices of all parameters [41]. This represents a significant improvement compared to the direct Monte Carlo simulation approach, representing a computational speedup of approximately 10^3 times compared to direct Monte Carlo simulation with 10^4 samples (1.1×10^5 evaluations). This efficiency gain enables practical sensitivity analysis of complex three-dimensional pipe systems in practical engineering applications.

In summary, the multiplicative dimensional reduction method approximation provides an efficient computational method for global sensitivity analysis of clamp-pipe systems by transforming high-dimensional integrals into products of one-dimensional components. This approach significantly reduces the computational burden associated with traditional Monte Carlo based methods, enabling practical sensitivity analysis for complex three-dimensional piping systems with multiple uncertain clamp parameters. The resulting computational efficiency, with speedup factors reaching three orders of magnitude compared to direct Monte Carlo simulation approaches, makes the multiplicative dimensional reduction method based

sensitivity analysis particularly valuable for engineering applications where computational resources are limited and rapid design iterations are required.

3.3 Numerical Algorithm and Implementation

The computational procedure for global sensitivity analysis of clamp-pipe systems quantifies the influence of clamp stiffness coefficients and installation position coordinates on natural frequency characteristics. The algorithm integrates three-dimensional Timoshenko beam finite element modeling with multiplicative dimensional reduction method based sensitivity analysis to efficiently evaluate the impact of clamp parameters. The procedure encompasses parameterized model construction, Timoshenko beam finite element based natural frequency analysis, and multiplicative dimensional reduction method approximations for Sobol' sensitivity indices.

As depicted in Algorithm 1, the NaFreSA procedure implementation begins with constructing a parameterized finite element model that explicitly incorporates clamp stiffness coefficients and installation position coordinates as the m-dimensional input parameter vector $\mathbf{x}$. The assembly process generates global mass and stiffness matrices that are explicit functions of these clamp parameters using the formulation in Eq. (10). Solving the resulting parameterized eigenvalue problem in Eq. (13) yields natural frequencies represented as $y_k(\mathbf{x})$ that explicitly depend on clamp configurations. The multiplicative dimensional reduction method based sensitivity analysis then efficiently computes both first-order and total-effect sensitivity indices for each of the m parameters by evaluating one-dimensional integrals along each parameter dimension. This computational procedure enables comprehensive identification of critical clamp parameters that most significantly influence the dynamic characteristics of complex piping systems, while maintaining computational efficiency through systematic dimension reduction.

Algorithm 1: Natural-frequency based sensitivity analysis (NaFreSA) of the clamp-pipe system

procedure NaFreSA**x**

Input: Clamp stiffness and position parameters $\mathbf{x} = [x_1, x_2, \ldots, x_m]^{\mathrm{T}}$;

Output: Natural frequencies and global sensitivity indices $\{y_k(\mathbf{x}), S_{i,k}, S_{\mathrm{T}i,k}\}$ $(k = 1, \cdots, n)$;

Step 1: Parameterized FE model construction

Model pipe segments using Timoshenko-beam elements;

Represent single clamps as distributed spring elements with stiffness coefficients;

Represent double clamps as coupled spring-mass systems with position coordinates;

Assemble global matrices using Eq. (10): $\mathbf{K}(\mathbf{x}) = \sum \mathbf{T}_e^{\mathrm{T}} \mathbf{K}^e(\mathbf{x}) \mathbf{T}_e$, $\mathbf{M}(\mathbf{x}) = \sum \mathbf{T}_e^{\mathrm{T}} \mathbf{M}^e(\mathbf{x}) \mathbf{T}_e$;

Step 2: Natural frequency analysis

Solve generalized eigenvalue problem using Eq. (13): $\mathbf{K}(\mathbf{x})\boldsymbol{\phi}^{(i)}(\mathbf{x}) = \Omega_i^2(\mathbf{x})\mathbf{M}(\mathbf{x})\boldsymbol{\phi}^{(i)}(\mathbf{x})$, and extract first n natural frequencies: $\{y_1(\mathbf{x}), \ldots, y_n(\mathbf{x})\}$;

Step 3: Global sensitivity analysis using M-DRM

Select reference point $\mathbf{x}_0$ of the uncertain vector $\mathbf{x}$;

for each uncertain parameter x_i **do**

Evaluate the one-dimensional integral via the Gauss-quadrature scheme for $\rho_{i,k} = \sum_{l=1}^{p} w_l \mathcal{M}_{k,i}(z_l, \mathbf{x}_{0,-i})$ and $\theta_{i,k} = \sum_{l=1}^{p} w_l [\mathcal{M}_{k,i}(z_l, \mathbf{x}_{0,-i})]^2$ in Eqs. (21) and (22);

end for

Compute sensitivity indices for k-th natural frequency using Eqs. (24) and (25):

$$S_{i,k} = \frac{\theta_{i,k}/\rho_{i,k}^2 - 1}{(\prod_{j=1}^{m} \theta_{j,k}/\rho_{j,k}^2) - 1} \text{ and } S_{\mathrm{T}i,k} = \frac{1 - \rho_{i,k}^2/\theta_{i,k}}{1 - (\prod_{j=1}^{m} \rho_{j,k}^2/\theta_{j,k})}$$

(Continued)

Algorithm 1 (continued)

Return: $\{y_k(\mathbf{x}), S_{i,k}, S_{\mathrm{T}i,k}; k = 1, \cdots, n\}$.
end procedure

In summary, the proposed NaFreSA algorithm provides a computationally efficient method for global sensitivity analysis of clamp-pipe systems. By integrating parameterized Timoshenko beam finite element modeling with multiplicative dimensional reduction method based sensitivity computation, the algorithm achieves an optimal balance between accuracy and efficiency essential for practical engineering applications. The evaluation of both first-order and total-effect sensitivity indices enables comprehensive assessment of clamp parameter importance for natural frequency predictions. The resulting sensitivity analysis supports informed decision-making in design optimization and uncertainty quantification of engine piping systems, making it a valuable tool for engineering practitioners and researchers in structural dynamics and vibration analysis.

4 Natural Frequency Based Sensitivity Analysis of Clamp Parameters

This section focuses on two representative pipe configurations, including a Z-shaped pipe and a spatial series-parallel pipe system, to demonstrate the methodology and reveal the relative importance of different clamp parameters. These configurations represent common structural layouts encountered in aerospace engine applications. Through sensitivity analysis, the investigation aims to identify critical clamp parameters that most significantly influence natural frequency characteristics, providing valuable insights for understanding piping systems with uncertain stiffness and installation position parameters.

4.1 A Planar Z-Shape Clamp-Pipe System

Consider the Z-shaped pipe model illustrated in Fig. 4. Control point coordinates of Z-shaped pipe are given as $P_1 = (0, 0, 0)$ mm, $P_2 = (300, 0, 0)$ mm, $P_3 = (300, 400, 0)$ mm, and $P_4 = (800, 400, 0)$ mm. Bending radius of the Z-shape pipe is 24 mm, whereas the outer and inner diameters of the pipe section are 8.0 and 6.4 mm, respectively. Specifically, positions of the single clamps to fix the Z-shape pipe system are defined as $C_1 = (100, 0, 0)$ mm, $C_2 = (300, 200, 0)$ mm, $C_3 = (500, 400, 0)$ mm. This allows one to develop an experimental model for natural frequency analysis of the pipe as presented in Fig. 5.

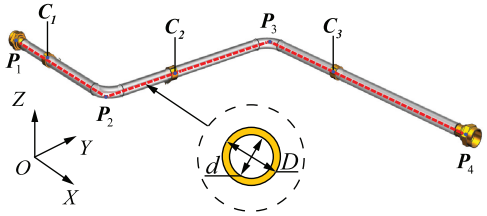

Figure 4: The geometry model of a Z-shape pipe system.

The Z-shaped pipe represents a typical aero-engine fuel pipe segment. The material is AISI 304 stainless steel with a Young's modulus of 200 GPa, density of 7800 kg/m^3, and Poisson's ratio of 0.3. The pipe has an outer diameter of 8.0 mm and an inner diameter of 6.4 mm, corresponding to a standard aerospace wall thickness. A bending radius of 24 mm ensures a smooth flow path and mitigates stress concentration. These parameters align with industrial design standards and are validated by experimental data from similar configurations.

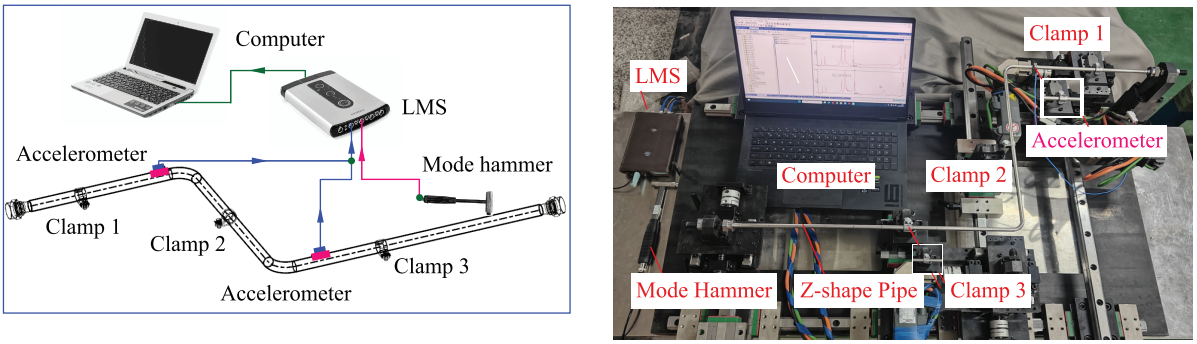

(a) Testing system **(b)** Physical setup

Figure 5: An illustration of the z-shape pipe system for experimental test results of the natural frequency.

The boundary conditions consist of three single clamps (C_1, C_2, C_3) modeled as six-degree-of-freedom elastic supports. At each clamp, distributed spring elements provide translational stiffness in the y- and z-directions (k_{iy}, k_{iz}) and rotational stiffness about the x-axis. The pipe ends are free, creating a statically indeterminate system where clamp positions critically influence natural frequencies by altering effective span lengths and boundary stiffness distributions. The stiffness values are derived from experimental measurements as detailed in Section 2.2, ensuring a realistic representation of clamp behavior in aerospace applications.

4.1.1 Experimental Verification

Fig. 5 shows a Z-shaped pipe supported by three clamps on a rigid frame. Two piezoelectric accelerometers (PCB 356A01) measure the dynamic response for identifying natural frequencies and mode shapes. A modal-impact hammer delivers impulse excitation across the relevant frequency range. The LMS SCADAS data acquisition system records the input force and acceleration signals. The numerical model uses Timoshenko beam elements for the pipe and spring elements for the clamps. The finite element model contains 298 nodes and 297 elements, yielding 1788 degrees of freedom. Validation uses Sensor Point 1 at $A_1(75, 0, 0)$ between Clamp 1 and Clamp 2, and Sensor Point 2 at $A_2(325, 400, 0)$.

Table 1 compares the first ten natural frequencies from simulation and experiment. All relative errors are within ±4%, indicating high model fidelity. The maximum deviation is 3.86% at the eighth mode f_{n8}; other modes show errors below 2%. This validates the modeling approach for capturing the dynamic characteristics of the Z-shaped pipe system and demonstrates the effectiveness of the Timoshenko beam and spring element formulation for clamp boundaries. The minor discrepancies within 4% arise from several sources. The numerical model assumes ideal clamp boundary conditions, but real clamps exhibit slight contact imperfections. Finite element discretization also introduces minor errors, especially at curved segments. The validation confirms that the method provides sufficient accuracy for engineering applications while maintaining computational efficiency.

Table 1: Comparison of the first-ten natural frequencies between simulation and experimental results.

Frequency (Hz)	f_{n1}	f_{n2}	f_{n3}	f_{n4}	f_{n5}	f_{n6}	f_{n7}	f_{n8}	f_{n9}	f_{n10}
Experiment	130.26	192.24	316.66	441.08	457.40	618.36	644.56	719.42	763.59	936.97
Simulation	129.31	195.52	314.62	441.80	452.94	617.82	647.31	747.22	771.93	957.04
Relative Error (%)	0.74%	1.69%	−0.65%	0.16%	0.98%	−0.09%	0.43%	3.86%	1.09%	2.14%

Fig. 6 presents the experimental frequency response functions, identifying the first ten natural frequencies of the Z-shaped pipe system. The FRF peaks align with the natural frequencies in Table 1, confirming the reliability of the experimental and numerical results. The agreement between simulation and experiment across a wide frequency range demonstrates the finite element model's accuracy in representing the physical behavior of the pipe system, including the effects of clamp stiffness and positioning on dynamic characteristics. This validated model provides a reliable basis for subsequent sensitivity analysis of clamp parameter uncertainties on natural frequencies.

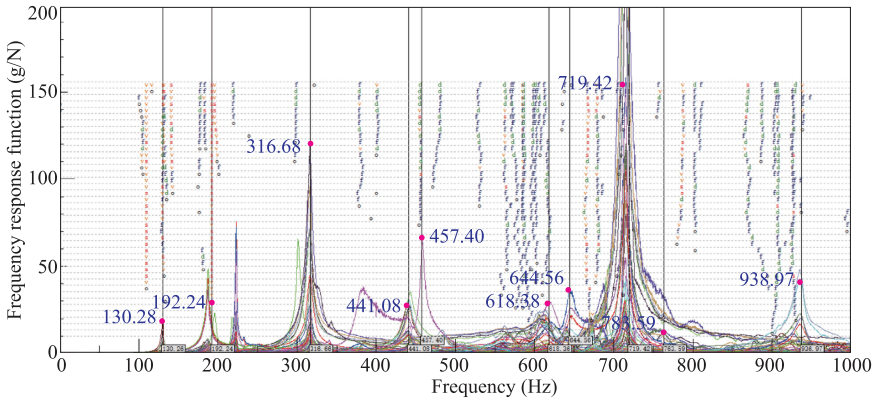

Figure 6: The experimental frequency response function (FRF) for natural frequency results of the Z-shaped pipe system.

4.1.2 Uncertain Clamp Parameters and Global Sensitivity Results

To simulate the natural vibration characteristics of the Z-shaped pipe, the stiffness coefficients k_{iy} and k_{iz} for each clamp are modeled as Lognormal random variables, while the clamp positions are treated as Gaussian random variables. Together with the uncertain bending radius, the probabilistic characteristics of all uncertain parameters are summarized in Table 2.

Table 2: Random variables are used to define probability characteristics of the Z-shape clamp-pipe system.

Physical Parameter	Random Variable	Distribution	Mean	Standard Deviation
Stiffness of Clamp 1	k_{1y} ($\times 10^3$ N/mm)	Lognormal	6.789	1.358
	k_{1z} ($\times 10^3$ N/mm)	Lognormal	3.923	0.7846
Stiffness of Clamp 2	k_{2y} ($\times 10^3$ N/mm)	Lognormal	6.789	1.358
	k_{2z} ($\times 10^3$ N/mm)	Lognormal	3.923	0.7846
Stiffness of Clamp 3	k_{3y} ($\times 10^3$ N/mm)	Lognormal	6.789	1.358
	k_{3z} ($\times 10^3$ N/mm)	Lognormal	3.923	0.7846
Clamp position	Clamp 1: C_1 (mm)	Gaussian	100	5.0
	Clamp 2: C_2 (mm)	Gaussian	200	10.0
	Clamp 3: C_3 (mm)	Gaussian	500	25.0
Geometric parameter	Bend radius R (mm)	Gaussian	24	1.2

Stiffness parameters follow a Lognormal distribution, which ensures positive values and captures the right-skewed variability arising from manufacturing processes and material scatter. This distribution aligns

with the asymmetric variability observed in experimental clamp data. Positional accuracy degrades with increasing distance from the reference due to cumulative assembly errors. Consequently, Clamp 1, located near the fixed end, exhibits the smallest variation, while Clamp 3, at the distal end, shows the largest variation of 25%. These values correspond to typical installation tolerances ranging from ±5 to ±25 mm in complex three-dimensional routing. The selected variation ranges ensure that the sensitivity analysis covers realistic scenarios without introducing overly conservative bounds that could obscure parameter importance rankings.

4.1.3 Results for the Global Sensitivity Analysis

Global sensitivity analysis of the Z-shaped pipe system uses the multiplicative dimension reduction method and Sobol' indices to quantify the influence of clamp stiffness and position parameters on natural frequencies. Twelve uncertain parameters are considered, including six clamp stiffness coefficients and four position variables. For the first ten natural frequencies, the method computes first-order and total-effect sensitivity indices by evaluating one-dimensional integrals along each parameter dimension. The parameterized finite element model from Section 2 incorporates these parameters through stiffness matrices and geometric mapping. Sensitivity indices are computed via Eqs. (24) and (25), enabling efficient assessment of parameter importance and interactions for the planar Z-shaped pipe configuration.

Table 3 presents the first-order sensitivity indices for twelve uncertain parameters across the first ten natural frequencies of the Z-shaped pipe system. Parameter influence varies systematically with modal order. Lower-order modes f_{n1} to f_{n5} are dominated by the third clamp position C_3, with sensitivity values exceeding 0.90 and reaching 0.996 for f_{n5}. This indicates that C_3 governs the fundamental modal characteristics, while all stiffness parameters contribute negligibly below 0.1%. The contrast demonstrates that lower-frequency dynamic response is primarily determined by spatial constraint configuration rather than local elastic properties.

Table 3: Results of the sensitivity index $S_{1i}^{(k)}$ for the first-ten natural frequencies of the Z-shape pipe system.

Mode	Clamp Stiffness						Clamp Location			Radius
	k_{1y}	k_{1z}	k_{2y}	k_{2z}	k_{3y}	k_{3z}	C_1	C_2	C_3	R
f_{n1}	<0.1%	<0.1%	<0.1%	0.052	<0.1%	<0.1%	0.032	<0.1%	0.904	<0.1%
f_{n2}	<0.1%	0.002	<0.1%	<0.1%	<0.1%	0.005	0.030	0.013	0.951	<0.1%
f_{n3}	0.002	<0.1%	<0.1%	<0.1%	0.005	<0.1%	0.031	<0.1%	0.960	<0.1%
f_{n4}	<0.1%	<0.1%	<0.1%	<0.1%	<0.1%	0.007	<0.1%	<0.1%	0.993	<0.1%
f_{n5}	<0.1%	<0.1%	<0.1%	<0.1%	0.004	<0.1%	<0.1%	<0.1%	0.996	<0.1%
f_{n6}	0.004	<0.1%	0.043	<0.1%	<0.1%	<0.1%	0.063	0.347	0.542	<0.1%
f_{n7}	<0.1%	0.005	0.003	0.016	<0.1%	0.002	0.082	0.218	0.674	<0.1%
f_{n8}	<0.1%	0.1%	<0.1%	0.015	<0.1%	0.004	0.018	0.036	0.924	<0.1%
f_{n9}	<0.1%	<0.1%	0.005	<0.1%	0.003	<0.1%	0.009	0.044	0.937	<0.1%
f_{n10}	<0.1%	0.015	<0.1%	0.004	<0.1%	0.013	0.153	0.055	0.755	0.004

As mode order increases beyond f_{n5}, the influence pattern changes. Although C_3 remains influential, its sensitivity gradually decreases from 0.996 at f_{n5} to 0.755 at f_{n10}. During this transition, C_2 becomes significant, with sensitivity increasing from 0.347 at f_{n6} to 0.218 at f_{n7} before slightly declining. Simultaneously, C_1 gains relevance in higher modes, reaching 0.153 at f_{n10} after negligible values in the first five

modes. This progressive shift from C_3 dominance to distributed sensitivity reflects the increasing complexity of higher-order vibration modes.

Stiffness parameters exhibit minimal influence. Only k_{2z} contributes 0.043 at f_{n6}, and k_{3z} registers 0.007 at f_{n4}. The bend radius R shows negligible impact across all modes, with a marginal 0.004 at f_{n10}, confirming that geometric curvature plays an insignificant role in determining natural frequencies. This systematic variation in parameter importance provides valuable insights for aerospace piping system design, where specific frequency ranges require targeted attention to clamp positioning accuracy.

4.2 A Spatial Series-Parallel Pipe System

Previous analyses of planar pipe systems have demonstrated that clamp position parameters dominate natural frequency characteristics compared to stiffness parameters. This finding motivates the current investigation into positional uncertainty effects in three-dimensional configurations in Fig. 7. The geometric configuration is based on actual routing data in Table 4. A three-dimensional finite element model is developed comprising 681 Timoshenko beam elements, 683 nodes, and 4098 degrees of freedom, enabling accurate simulation of natural vibration modes. Flexible pipe segments are represented by beam elements, while clamp constraints are modeled via spring elements. This approach captures the influence of clamp installation deviations on system stiffness and boundary conditions, providing a reliable basis for assessing the impact of positional uncertainties on dynamic response.

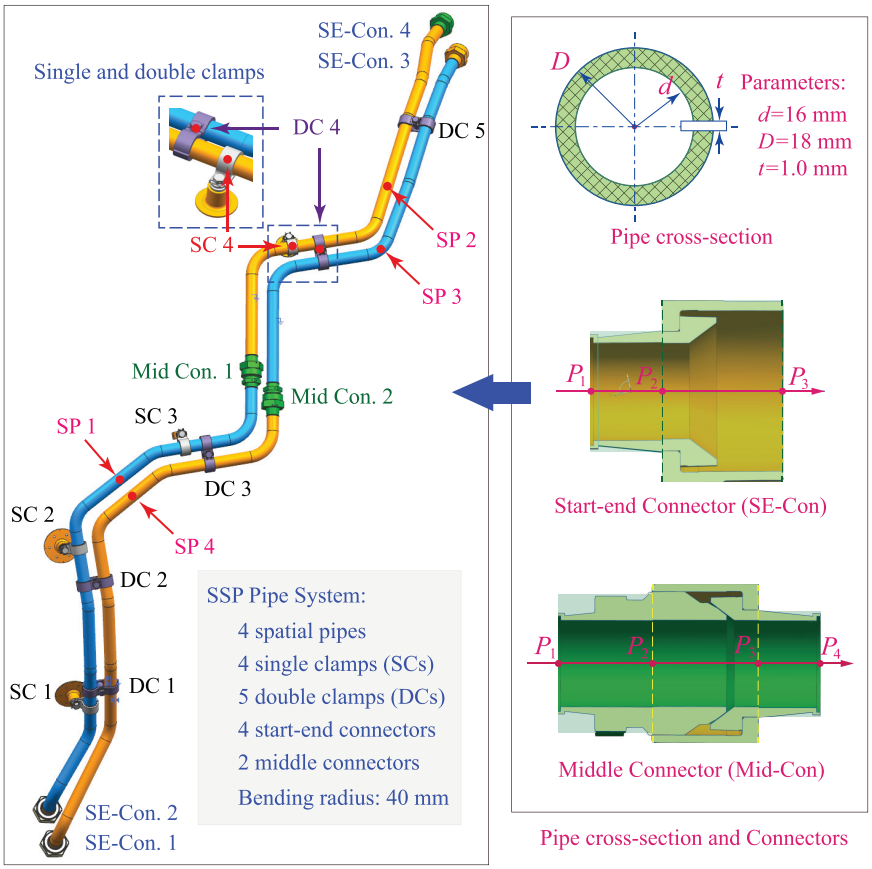

Figure 7: An illustration of the spatial serial-parallel (SSP) pipe system: Four SSP pipes, two middle connectors (Mid-Cons), four start-end connectors (SE-Cons), four single clamps (SCs), and five double clamps (DCs).

Table 4: Control point coordinates of series-parallel spatial pipe systems.

Point ID.	P_1	P_2	P_3	P_4	P_5	P_6	P_7	P_8
X (mm)	−25.17	−67.54	−127.54	−219.74	−308.10	−306.63	−420.07	−452.44
Y (mm)	1757.41	1733.04	1697.09	1644.95	1583.12	1419.55	1386.38	1376.92
Z (mm)	−558.16	−556.05	−532.18	−487.39	−431.54	−432.39	−309.40	−274.30
Point ID.	P_9	P_{10}	P_{11}	P_{12}	P_{13}	P_{14}	P_{15}	P_{16}
X (mm)	−489.62	−489.62	−492.63	−522.61	−521.55	−486.35	−523.81	−487.51
Y (mm)	1366.0	1201.6	1096.5	1101.3	1098.1	1097.3	1004.5	1004.5
Z (mm)	−233.99	−233.99	−162.85	−50.94	57.83	189.20	324.96	360.12
Point ID.	P_{17}	P_{18}	P_{19}	P_{20}	P_{21}	P_{22}	P_{23}	P_{24}
X (mm)	81.45	39.67	−52.57	−113.22	−284.40	−282.79	−391.92	−426.00
Y (mm)	1734.6	1734.6	1705.7	1670.8	1573.9	1394.4	1363.0	1353.2
Z (mm)	−553.07	−559.18	−556.97	−533.25	−450.09	−451.03	−344.26	−310.92
Point ID.	P_{25}	P_{26}	P_{27}	P_{28}	P_{29}	P_{30}	P_{31}	P_{32}
X (mm)	−476.87	−476.87	−487.01	−522.94	−520.24	−485.62	−498.04	−451.33
Y (mm)	1705.7	1338.5	1192.6	1065.5	1071.3	1068.1	1004.5	1004.5
Z (mm)	−261.15	−261.15	−183.83	−49.74	59.80	189.03	277.52	322.77

Table 5 compares the first ten natural frequencies from finite element simulation and experimental testing. The relative errors all fall within ±3%, demonstrating the high fidelity of the numerical model. The maximum deviation occurs at the sixth mode f_{n6}, where the simulation underestimates the frequency by 2.93%. Most other modes agree within 1%. This validation confirms the accuracy of the modeling approach in capturing the dynamic characteristics of the spatial series-parallel piping system and its suitability for subsequent sensitivity analysis of clamp position effects.

Table 5: Comparison of the first ten natural frequencies between simulation and experimental results.

Frequency (Hz)	f_{n1}	f_{n2}	f_{n3}	f_{n4}	f_{n5}	f_{n6}	f_{n7}	f_{n8}	f_{n9}	f_{n10}
Experiment	130.42	175.24	208.98	229.37	245.64	279.50	298.10	317.67	330.12	369.06
Simulation	131.59	175.38	205.85	225.94	243.30	271.29	300.27	317.87	336.42	377.88
Relative Error (%)	0.89	0.08	−1.49	−1.49	−0.95	−2.93	0.072	0.063	1.91	2.39

Fig. 8 displays the experimentally obtained frequency response functions, which identify the first ten natural frequencies of the spatial series-parallel pipe system. The FRF peaks align with the natural frequencies listed in Table 5, validating both the experimental measurements and numerical predictions. The close agreement across a wide frequency range demonstrates that the finite element model accurately captures the physical behavior of the pipe system, including the influence of clamp positioning on its dynamics. This validated model provides a basis for the subsequent global sensitivity analysis of clamp position uncertainties.

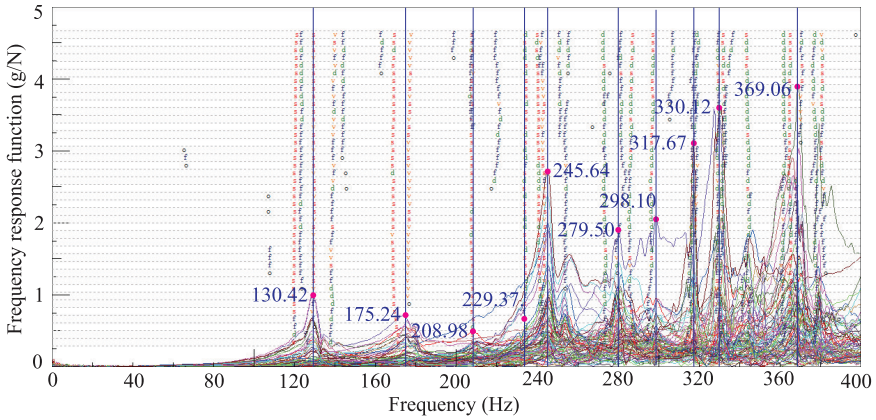

Figure 8: The experimental frequency response function (FRF) for natural frequency results of the SSP pipe system.

4.2.1 The Deviation Effect of Double Clamps

Double clamps connect and secure parallel pipe sections, enhancing the overall structural stiffness. This study investigates how installation position deviations of double clamps influence the system's vibration characteristics. Controlled deviations of ±15 mm with 1 mm increments are applied to each of the five double clamps. A full factorial design evaluates their effects on the first ten natural frequencies.

Fig. 9 shows the variations of the first four natural frequencies with installation deviations. Different clamps dominate the response in different modes, revealing a mode-dependent sensitivity pattern. For the first mode, DC-4 shows a pronounced nonlinear decrease while DC-3 increases linearly. DC-1, DC-2, and DC-5 show negligible variation. For the second mode, DC-3 increases and DC-4 decreases significantly, with DC-1 remaining constant. DC-2 and DC-5 show minor effects. The third mode is dominated by DC-2 which increases and DC-4 which decreases, while DC-1 and DC-3 remain stable. For the fourth mode, DC-4 again dominates with a steep decline and DC-2 increases moderately. DC-1 is invariant and DC-3 and DC-5 have limited influence.

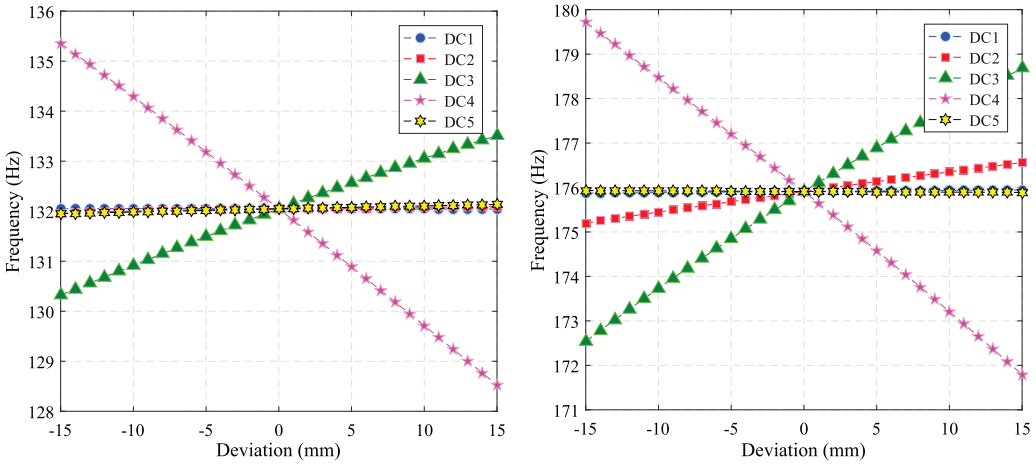

(a) The first-order natural frequency

(b) The second-order natural frequency

Figure 9: (Continued)

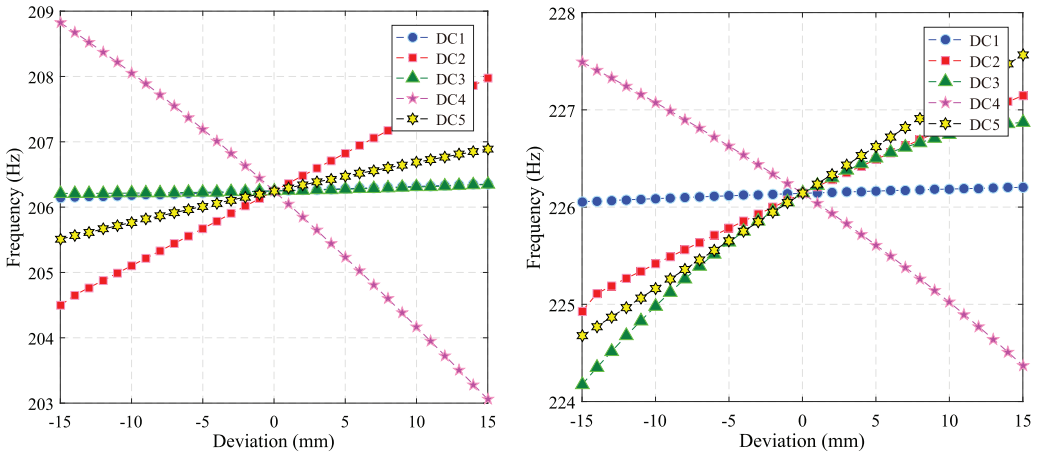

(c) The third-order natural frequency **(d)** The fourth-order natural frequency

Figure 9: Numerical variations of the natural frequency result as the position deviation within the interval $[-15, 15]$ mm for each double clamp individually (one-at-a-time analysis).

DC-4 consistently shows the highest sensitivity across all four modes, indicating its critical role. DC-3 also exhibits significant influence in multiple modes. In contrast, DC-1 remains insensitive, suggesting minimal impact. DC-2 and DC-5 show moderate influence that depends on the mode. These findings identify DC-4 and DC-3 as key clamps governing system vibrations, while DC-1 can be assigned relaxed tolerance controls.

Table 6 summarizes the natural frequency ranges induced by ±15 mm installation deviations for each double clamp. DC-4 exhibits the largest influence, particularly in the eighth mode at 24.14 Hz, the sixth mode at 10.10 Hz, and the third mode at 5.76 Hz. DC-3 also shows substantial impact, primarily in the seventh mode at 10.72 Hz, the tenth mode at 12.16 Hz, and the second mode at 6.14 Hz. DC-2 has notable effects on the ninth mode at 14.63 Hz and the third mode at 3.48 Hz. In contrast, DC-1 and DC-5 show minimal influence across most modes. These results confirm DC-4 and DC-3 as the primary contributors to frequency variations, while DC-1 and DC-5 are low-sensitivity components suitable for relaxed tolerance control.

Table 6: The min-max range of natural frequency results caused by installation deviations of double clamps.

Frequency Order	f_{n1}	f_{n2}	f_{n3}	f_{n4}	f_{n5}	f_{n6}	f_{n7}	f_{n8}	f_{n9}	f_{n10}
DClamp 1 (Hz)	<0.1	<0.1	0.21	0.15	<0.1	0.48	0.55	0.12	0.15	2.67
DClamp 2 (Hz)	0.14	1.37	3.48	2.22	2.64	2.94	0.66	2.31	14.63	2.14
DClamp 3 (Hz)	3.19	6.14	0.14	2.70	8.16	5.61	10.72	3.88	0.50	12.16
DClamp 4 (Hz)	6.83	7.92	5.76	3.12	1.23	10.10	2.86	24.14	4.52	1.06
DClamp 5 (Hz)	0.19	<0.1	1.38	2.89	1.48	0.63	<0.1	0.97	2.41	0.22

4.2.2 Global Sensitivity Analysis Results

A global sensitivity analysis based on Sobol indices quantifies the influence of double-clamp position deviations on the natural frequencies of the spatial series-parallel piping system. Unlike local sensitivity methods, which evaluate parameter effects at a single nominal point, the Sobol method accounts for the full range of parameter variations and their nonlinear interactions across the entire input domain. This approach

comprehensively assesses how each clamp location contributes to the variability in system response and identifies which positional uncertainties most significantly affect critical vibration modes.

Sobol sensitivity indices decompose the total variance of the natural frequencies into contributions from individual input parameters and their interactions. First-order indices measure the main effect of each clamp position, while total-effect indices include both direct effects and all interaction terms. This decomposition clarifies the relative importance of different clamp locations and reveals potential synergistic effects. The Sobol sensitivity indices for the first ten natural frequencies are presented in Table 7 and Fig. 10.

Table 7: Sobol sensitivity indices for the first ten natural frequencies of the spatial series-parallel piping system.

Mode	f_{n1}	f_{n2}	f_{n3}	f_{n4}	f_{n5}	f_{n6}	f_{n7}	f_{n8}	f_{n9}	f_{n10}
DC-1	<0.1%	<0.1%	<0.1%	<0.1%	<0.1%	<0.1%	<0.1%	<0.1%	<0.1%	0.0288
DC-2	<0.1%	0.0148	0.1622	0.1597	0.1401	0.0357	<0.1%	0.0195	0.861	0.0335
DC-3	0.1881	0.4753	<0.1%	0.3411	0.8216	0.2833	0.9851	0.0196	<0.1%	0.9266
DC-4	0.8113	0.5097	0.806	0.2225	0.0247	0.6791	0.0114	0.9605	0.1285	<0.002
DC-5	<0.1%	<0.1%	0.0312	0.2757	0.0133	<0.1%	<0.1%	<0.1%	0.011	<0.1%

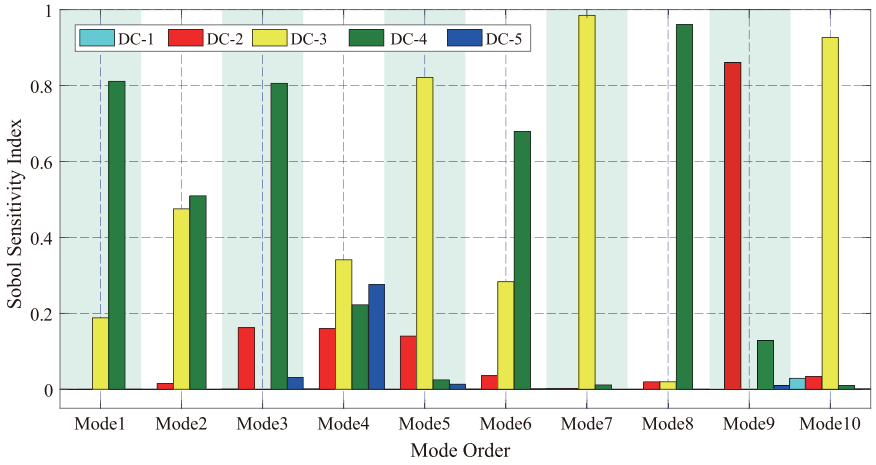

Figure 10: Sobol sensitivity indices for double-clamp positions across the first ten natural frequencies.

The results demonstrate significant variation in the influence of different double-clamp positions. Clamp DC-4 exhibits the highest sensitivity across several modes, with indices of 0.8113 for f_{n1}, 0.806 for f_{n3}, and 0.9605 for f_{n8}. Clamp DC-3 strongly influences higher-order modes, with indices of 0.8216 for f_{n5}, 0.9851 for f_{n7}, and 0.9266 for f_{n10}. In contrast, clamps DC-1 and DC-5 show minimal impact, with sensitivity indices below 0.03 for nearly all frequencies. The exception is DC-1 at f_{n10} with an index of 0.0288. Clamp DC-2 presents a moderate influence, notably on f_{n3} (0.1622) and f_{n4} (0.1597), yet its overall contribution remains secondary to DC-3 and DC-4.

These sensitivity findings are consistent with the earlier single-parameter deviation analysis presented in Fig. 9 and Table 6. That analysis identified DC-4 as inducing the largest frequency shifts, quantified here by its high Sobol indices. Both methods confirm DC-3 as highly influential for higher-order modes and DC-1 as negligible. This mutual validation strengthens the conclusion that DC-4 and DC-3 are the primary determinants of the system's dynamic behavior, whereas the positions of DC-1 and DC-5 can be governed by relaxed tolerance specifications.

The non-uniform distribution of parameter sensitivity underscores the importance of targeted design optimization. Tighter manufacturing and installation tolerances should be applied to high-sensitivity clamps such as DC-3 and DC-4. Focusing quality control efforts on these critical components provides a direct pathway to enhance structural robustness and mitigate resonance risk under operational conditions.

In summary, the global sensitivity analysis reveals a highly non-uniform influence of double-clamp positioning on the system's natural frequencies. Clamp DC-4 is the most critical parameter across multiple modes. Clamp DC-3 exerts substantial influence on higher-order modes. Clamps DC-1 and DC-5 have a minimal impact, and DC-2 shows a moderate, mode-specific influence. This establishes a clear hierarchy of parameter importance, demonstrating that geometric uncertainties in clamp positioning dominate the dynamic response. Consequently, tolerance requirements can be strategically relaxed for less sensitive clamp locations without significantly compromising system performance.

5 Conclusions

This study develops an efficient method for global sensitivity analysis of aero-engine pipe systems with uncertain clamp support conditions. The approach combines a three-dimensional Timoshenko beam finite-element model with the multiplicative dimensional reduction method to compute Sobol' sensitivity indices rapidly. The computational cost is reduced by three orders of magnitude compared with conventional Monte Carlo simulation while preserving accuracy.

Numerical examples on a planar Z-shaped pipe and a spatial series-parallel configuration validate the method. For the Z-shaped pipe, the position of clamp C_3 dominates the first five natural frequencies (Sobol' indices > 0.9), while stiffness parameters have negligible influence (<0.1%). In the spatial system, double clamps DC-4 and DC-3 are critical, with indices exceeding 0.8 for multiple modes. These results show that geometric uncertainties in clamp positioning govern the dynamic response, whereas local stiffness variations have minimal global effect. Note that the utility of natural frequency results alone cannot establish a complete evaluation criterion for clamp characteristics. A more robust selection criterion based on local stress amplitudes and high-cycle fatigue damage can be further implemented to determine the critical stiffness components or position deviations for clamp selections.

In summary, the work contributes an efficient computational procedure for sensitivity analysis of high-dimensional clamp parameters in piping systems. The results establish a clear hierarchy of parameter importance, demonstrating that positional accuracy of specific clamps is paramount. This insight allows strategic allocation of manufacturing tolerances, focusing precision on dominant parameters without compromising dynamic performance. The method supports practical design and maintenance decisions for aero-engine pipes. It enables optimized tolerance assignment, guides inspection priorities, and facilitates rapid evaluation of design alternatives. By identifying the most influential clamp parameters, the approach can be expected to enhance system reliability and reduce lifecycle costs while maintaining safety.

Acknowledgement: None.

Funding Statement: This research was funded by the Major Projects of Aero-Engines and Gas Turbines grant number J2019-I-0008-0008.

Author Contributions: The authors confirm contribution to the paper as follows: study conception and design: Yan Shi, Xufang Zhang; data collection: Yan Shi, Shang Ren; analysis and interpretation of results: Yan Shi, Xin Wang, Yi Wang; draft manuscript preparation: Yan Shi, Bingfeng Zhao and Xufang Zhang. All authors reviewed and approved the final version of the manuscript.

Availability of Data and Materials: Data available on request from the authors.

Ethics Approval: Not applicable.

Conflicts of Interest: The authors declare no conflicts of interest.

Appendix A The Local Mass and Stiffness Matrices

The local mass matrix $\mathbf{M}_{11}^{e}$ requires correction in the off-diagonal terms to maintain consistency with the shape function integration results. The corrected matrix is expressed as

$$\mathbf{M}_{11}^{e}=\rho AL\begin{bmatrix}\frac{1}{3} & 0 & 0 & 0 & 0 & 0\\ 0 & \frac{13}{35}+\frac{6I_z}{5AL^2} & 0 & 0 & 0 & \frac{11L}{210}+\frac{I_z}{10AL}\\ 0 & 0 & \frac{13}{35}+\frac{6I_y}{5AL^2} & 0 & -\frac{11L}{210}+\frac{I_y}{10AL} & 0\\ 0 & 0 & 0 & \frac{J}{3A} & 0 & 0\\ 0 & 0 & -\frac{11L}{210}+\frac{I_y}{10AL} & 0 & \frac{L^2}{105}+\frac{2I_y}{15A} & 0\\ 0 & \frac{11L}{210}+\frac{I_z}{10AL} & 0 & 0 & 0 & \frac{L^2}{105}+\frac{2I_z}{15A}\end{bmatrix}. \tag{A1}$$

Similarly, the coupling mass matrix $\mathbf{M}_{21}^{e}$ requires corrections in the signs of the shear coupling terms and the rotational inertia terms. The corrected matrix is expressed as

$$\mathbf{M}_{21}^{e}=\mathbf{M}_{12}^{e\mathrm{T}}=\rho AL\begin{bmatrix}\frac{1}{6} & 0 & 0 & 0 & 0 & 0\\ 0 & \frac{9}{70}+\frac{6I_z}{5AL^2} & 0 & 0 & -\frac{13L}{420}+\frac{I_z}{10AL} & 0\\ 0 & 0 & \frac{9}{70}+\frac{6I_y}{5AL^2} & 0 & 0 & \frac{13L}{420}-\frac{I_y}{10AL}\\ 0 & 0 & 0 & \frac{J}{6A} & 0 & 0\\ 0 & \frac{13L}{420}-\frac{I_z}{10AL} & 0 & 0 & -\frac{L^2}{140}-\frac{I_z}{15A} & 0\\ 0 & 0 & -\frac{13L}{420}+\frac{I_y}{10AL} & 0 & 0 & -\frac{L^2}{140}-\frac{I_y}{15A}\end{bmatrix}. \tag{A2}$$

The stiffness matrices $\mathbf{K}_{11}^{e}$ and $\mathbf{K}_{21}^{e}$ are correctly formulated and maintain consistency with the Timoshenko beam theory and previous derivations. The local stiffness matrix $\mathbf{K}_{11}^{e}$ is expressed as

$$\mathbf{K}_{11}^{e}=\frac{1}{L^3}\begin{bmatrix}EAL^2 & 0 & 0 & 0 & 0 & 0\\ 0 & \frac{12EI_z}{1+P_z} & 0 & 0 & 0 & \frac{6EI_zL}{1+P_z}\\ 0 & 0 & \frac{12EI_y}{1+P_y} & 0 & -\frac{6EI_yL}{1+P_y} & 0\\ 0 & 0 & 0 & GJL^2 & 0 & 0\\ 0 & \frac{6EI_zL}{1+P_z} & 0 & 0 & \frac{EI_yL^2(4+P_y)}{1+P_y} & 0\\ 0 & 0 & -\frac{6EI_yL}{1+P_y} & 0 & 0 & \frac{EI_zL^2(4+P_z)}{1+P_z}\end{bmatrix} \tag{A3}$$

and the coupling stiffness matrix $\mathbf{K}_{21}^{e}$ is expressed as

$$\mathbf{K}_{21}^{e} = \mathbf{K}_{12}^{e\mathrm{T}} = \begin{bmatrix} -\frac{EA}{L} & 0 & 0 & 0 & 0 & 0 \\ 0 & -\frac{12EI_z}{L^3(1+P_z)} & 0 & 0 & 0 & -\frac{6EI_z}{L^2(1+P_z)} \\ 0 & 0 & -\frac{12EI_y}{L^3(1+P_y)} & 0 & \frac{6EI_y}{L^2(1+P_y)} & 0 \\ 0 & 0 & 0 & -\frac{GJ}{L} & 0 & 0 \\ 0 & \frac{6EI_z}{L^2(1+P_z)} & 0 & 0 & \frac{EI_y(2-P_y)}{L(1+P_y)} & 0 \\ 0 & 0 & -\frac{6EI_y}{L^2(1+P_y)} & 0 & 0 & \frac{EI_z(2-P_z)}{L(1+P_z)} \end{bmatrix}, \tag{A4}$$

in which the shear deformation parameters are defined as $P_y = \frac{12EI_y}{\kappa GAL^2}$ and $P_z = \frac{12EI_z}{\kappa GAL^2}$ for the circular pipe section.

References

1. Cao Y, Chen W, Ma H, Li H, Wang B, Tan L, et al. Dynamic modeling and experimental verification of clamp-pipeline system with soft nonlinearity. Nonlinear Dyn. 2023;111(19):17725–48. doi:10.1007/s11071-023-08814-y.
2. Zhangabay N, Bonopera M, Avramov K, Chernobryvko M, Buganova S. Use of scaled models to evaluate reinforcement efficiency in damaged main gas pipelines to prevent avalanche failure. Comput Model Eng Sci. 2025;145(1):241–61. doi:10.32604/cmes.2025.069544.
3. Ma Y, Wang Z, Zhang J, Huo R, Yuan X. Sensitivity analysis of electromagnetic scattering from dielectric targets with polynomial chaos expansion and method of moments. Comput Model Eng Sci. 2024;140(2):2079–102. doi:10.32604/cmes.2024.048488.
4. Zhang X, Wang L, Sørensen JD. AKOIS: an adaptive Kriging oriented importance sampling method for structural system reliability analysis. Struct Saf. 2020;82:101876.
5. Steltner K, Pedersen CB, Kriegesmann B. Semi-intrusive approach for stiffness and strength topology optimization under uncertainty. Optim Eng. 2023;24(3):2181–211. doi:10.1007/s11081-022-09770-z.
6. Li W, Liu Z, Ma Y, Meng Z, Ma J, Liu W, et al. Sensitivity analysis of structural dynamic behavior based on the sparse polynomial chaos expansion and material point method. Comput Model Eng Sci. 2025;142(2):1515–43. doi:10.32604/cmes.2025.059235.
7. Li F, Liu H, Li Y, Chen L, Lian H. Shape sensitivity analysis of acoustic scattering with series expansion boundary element methods. Comput Model Eng Sci. 2025;143(3):2785–809. doi:10.32604/cmes.2025.066001.
8. Cao Y, Chai Q, Guo X, Ma H, Wang P. Comparative study on two finite element models for multi-clamp pipeline system. J Mech Sci Technol. 2022;36(3):1157–69. doi:10.1007/s12206-022-0208-5.
9. Gao PX, Zhai JY, Yan YY, Han QK, Qu FZ, Chen XH. A model reduction approach for the vibration analysis of hydraulic pipeline system in aircraft. Aerosp Sci Technol. 2016;49(2):144–53. doi:10.1016/j.ast.2015.12.002.
10. Sun Z, Yu R, Wang X, Zhang X. Dynamic analysis of liquid-filled clamp-pipe systems based on the spectral element method. Arch Appl Mech. 2025;95(1):24. doi:10.1007/s00419-024-02723-1.
11. Xu H, Zhang X, Sun Z, Sun S. A Gegenbauer-polynomial-based semi-analytical approach for dynamic modeling of series-parallel pipe systems under elastic boundary conditions. Appl Math Model. 2025;149:116317. doi:10.1016/j.apm.2025.116317.
12. El-Sayed T, El-Mongy H. Free vibration and stability analysis of a multi-span pipe conveying fluid using exact and variational iteration methods combined with transfer matrix method. Appl Math Model. 2019;71:173–93. doi:10.1016/j.apm.2019.02.006.

13. Li Q, Yang K, Zhang L, Zhang N. Frequency domain analysis of fluid-structure interaction in liquid-filled pipe systems by transfer matrix method. Int J Mech Sci. 2002;44(10):2067–87. doi:10.1016/s0020-7403(02)00170-4.
14. Guo X, Ge H, Xiao C, Ma H, Sun W, Li H. Vibration transmission characteristics analysis of the parallel fluid-conveying pipes system: numerical and experimental studies. Mech Syst Signal Process. 2022;177(11):109180. doi:10.1016/j.ymssp.2022.109180.
15. Guo X, Cao Y, Ma H, Xiao C, Wen B. Dynamic analysis of an L-shaped liquid-filled pipe with interval uncertainty. Int J Mech Sci. 2022;217(1):107040. doi:10.1016/j.ijmecsci.2021.107040.
16. Chen W, Guo Z, Chen S, Cao Y, Guo X, Ma H, et al. Semi-analytic modeling and experimental verification of arbitrary aero-engine complex spatial pipeline. Appl Math Model. 2024;131(4):505–34. doi:10.1016/j.apm.2024.04.003.
17. Dou B, Luo ZB, Deng TC, Mao XY, Li M, Ding H. Two-directional and multi-modal vibration reduction of fluid-conveying pipes by using piecewise retaining clips. Thin-Walled Struct. 2025;209:112945. doi:10.1016/j.tws.2025.112945.
18. Chen W, Cao Y, Guo X, Ma H, Wen B, Wang B. Semi-analytical dynamic modeling and fluid-structure interaction analysis of L-shaped pipeline. Thin-Walled Struct. 2024;196(4):111485. doi:10.1016/j.tws.2023.111485.
19. Ma H, Sun W, Ji W, Zhang Y, Liu X, Liu H. Dynamic modeling and vibration analysis of planar pipeline with partial constrained layer damping treatment: theoretical and experimental studies. Compos Struct. 2023;323(1):117476. doi:10.1016/j.compstruct.2023.117476.
20. Bu Y, Tang Y, Yang T, Ding Q. Enhanced dynamic modeling of pipes conveying fluid with multiple constraints and accessories based on spectral element method. Mech Syst Signal Processing. 2025;237:113097.
21. Wang L, Yin Y, Qi L, Qu C, Yu Y, Liu B, et al. High frequency vibration calculation methods for PFCPs. Int J Mech Sci. 2025;301(4):110502. doi:10.1016/j.ijmecsci.2025.110502.
22. Bu Y, Tang Y, Wu J, Yang T, Ding Q, Li Y. Novel vibration suppression of spinning periodically acoustic black hole pipes based on the band-gap mechanism. Thin-Walled Struct. 2025;212(20):113198. doi:10.1016/j.tws.2025.113198.
23. Ji W, Ma H, Liu F, Sun W, Wang D. Dynamic analysis of cracked pipe elbows: numerical and experimental studies. Int J Mech Sci. 2024;281(1):109580. doi:10.1016/j.ijmecsci.2024.109580.
24. Chai Q, Zeng J, Hui M, Kun L, Qingkai H. A dynamic modeling approach for nonlinear vibration analysis of the L-type pipeline system with clamps. Chin J Aeronaut. 2020;33(12):3253–65. doi:10.1016/j.cja.2020.04.007.
25. Wang W, Zhou C, Gao H, Zhang Z. Application of non-probabilistic sensitivity analysis in the optimization of aeronautical hydraulic pipelines. Struct Multidiscip Optim. 2018;57(6):2177–91. doi:10.1007/s00158-017-1848-4.
26. Guan Y, Zhi P, Wang Z. A novel variable-fidelity kriging surrogate model based on global optimization for black-box problems. Comput Model Eng Sci. 2025;144(3):3343–68. doi:10.32604/cmes.2025.069515.
27. Amstutz S. Sensitivity analysis with respect to a local perturbation of the material property. Asymptot Anal. 2006;49(1–2):87–108. doi:10.3233/asy-2006-778.
28. Zhao Y, Cheng X, Zhang T, Wang L, Shao W, Wiart J. A global-local attention network for uncertainty analysis of ground penetrating radar modeling. Reliab Eng Syst Saf. 2023;234(2):109176. doi:10.1016/j.ress.2023.109176.
29. Borgonovo E. Sensitivity analysis with finite changes: an application to modified EOQ models. Eur J Oper Res. 2010;200(1):127–38.
30. Liu W, Cao G, Zhai HB, Liu YS. Sensitivity analysis and dynamic optimization design of supports' positions for engine pipelines. J Aerosp Power. 2012;27(12):2756–62. doi:10.2514/6.1994-4275.
31. Yao Z, Hao J, Tan Z, Li C, Zhao J. Ratcheting fatigue reliability and sensitivity analysis of hydraulic pipe under in-service loadings. Reliab Eng Syst Saf. 2025;264:111293. doi:10.1016/j.ress.2025.111293.
32. Hou J, Jiang Z, Wu F, Lian H, Wang Z, Liu Z, et al. A novel multi-objective topology optimization method for stiffness and strength-constrained design using the SIMP approach. Comput Model Eng Sci. 2025;144(2):1545–72. doi:10.32604/cmes.2025.068482.
33. Zhang X, Pandey MD. Structural reliability analysis based on the concepts of entropy, fractional moment and dimensional reduction method. Struct Saf. 2013;43(1):28–40. doi:10.1016/j.strusafe.2013.03.001.
34. Borgonovo E, Tarantola S, Plischke E, Morris MD. Transformations and invariance in the sensitivity analysis of computer experiments. J R Stat Soc Ser B Stat Methodol. 2014;76(5):925–47. doi:10.1111/rssb.12052.

35. Ye K, Qin L, Ye Z, Yang D, Dong B. Uncertainty analysis of rudder shaft thermal conditions on the flutter characteristics of the hypersonic control surface. Aerosp Sci Technol. 2024;155:109721. doi:10.2139/ssrn.4727103.
36. Wan HP, Todd MD, Ren WX. Statistical framework for sensitivity analysis of structural dynamic characteristics. J Eng Mech. 2017;143(9):04017093. doi:10.1061/(asce)em.1943-7889.0001314.
37. Guo Q, Liu Y, Zhao Y, Li B, Yao Q. Improved resonance reliability and global sensitivity analysis of multi-span pipes conveying fluid based on active learning Kriging model. Int J Press Vessel Pip. 2019;170(4):92–101. doi:10.1016/j.ijpvp.2019.01.016.
38. Li D, Jiang P, Hu C, Yan T. Comparison of local and global sensitivity analysis methods and application to thermal hydraulic phenomena. Prog Nucl Energy. 2023;158(3):104612. doi:10.1016/j.pnucene.2023.104612.
39. Saltelli A, Annoni P, Azzini I, Campolongo F, Ratto M, Tarantola S. Variance based sensitivity analysis of model output. Design and estimator for the total sensitivity index. Comput Phys Commun. 2010;181(2):259–70. doi:10.1016/j.cpc.2009.09.018.
40. Sobol IM. Global sensitivity indices for nonlinear mathematical models and their Monte Carlo estimates. Math Comput Simulation. 2001;55(1–3):271–80. doi:10.1016/s0378-4754(00)00270-6.
41. Zhang X, Pandey MD. An effective approximation for variance-based global sensitivity analysis. Reliab Eng Syst Safety. 2014;121(2):164–74. doi:10.1016/j.ress.2013.07.010.
42. Duong PLT, Tran TT, Raghavan N. Application of multiplicative dimensional reduction method for uncertainty quantification and sensitivity analysis of mems electrostatic actuators. Microelectron Reliab. 2017;76(5):619–25. doi:10.1016/j.microrel.2017.07.091.
43. Minh LQ, Duong PLT, Goncalves J, Kwok E, Lee M. A two-stage approach of multiplicative dimensional reduction and polynomial chaos for global sensitivity analysis and uncertainty quantification with a large number of process uncertainties. J Taiwan Inst Chem Eng. 2017;78(1):254–64. doi:10.1016/j.jtice.2017.06.012.
44. Balomenos GP, Genikomsou AS, Polak MA, Pandey MD. Efficient method for probabilistic finite element analysis with application to reinforced concrete slabs. Eng Struct. 2015;103(3):85–101. doi:10.1016/j.engstruct.2015.08.038.
45. Zhang X, Zhang Y, Pandey MD. Global sensitivity analysis of a CNC machine tool: application of MDRM. Int J Adv Manuf Technol. 2015;81(1):159–69. doi:10.1007/s00170-015-7128-9.